ICARUS 17, 443–456 (1972)

Mariner 9 Ultraviolet Spectrometer Experiment: Photometry and Topography of Mars

C. W. HORD, C. A. BARTH, AND A. I. STEWART

Department of Astro-Geophysics and Laboratory for Atmospheric and Space Physics, University of Colorado, Boulder, Colorado 80302

AND

A. L. LANE

Jet Propulsion Laboratory, California Institute of Technology, Pasadena, California 91103

Received June 7, 1972

Reflectance properties of Mars are measures in a 100-Å band centered at 3050 Å by the ultraviolet spectrometer. The instrument has an angular resolution which is equivalent to an area of 10 × 30 km on the surface of Mars. The transition from dusty conditions, which prevailed at the time of arrival of Mariner 9 on 14 November 1971, began on 1 January 1972, and relatively clear conditions existed after 23 January 1972. As the atmosphere became clearer, the scattering properties began to show a morning enhancement in both terminator and illuminated disk reflectance. A topographic map of Mars based on the scattering of ultraviolet light from the Mars atmosphere is shown. This map is based upon 3050-Å data obtained after the Mars atmosphere had cleared in the ultraviolet. Ultraviolet light which is Rayleigh-scattered by the Mars molecular atmosphere, with allowance for uniform turbidity, is proportional to surface pressure independent of atmospheric temperature structure. Comparison with Mariner 9 radio occultation measurements determines the fraction of total reflectance that is due to atmospheric scattering.

INTRODUCTION

Analysis of the reflectance of Mars in a 100-Å wavelength band centered at 3050 Å from ultraviolet spectrometers on the Mariner 6 and 7 spacecraft (Barth and Hord, 1971; Hord, 1972) shows this wavelength to be useful in describing the ultraviolet scattering properties of Mars. Variations in the intensity at 3050 Å were found to correlate with variations in local surface pressure, and ultraviolet surface albedo changes were negligible to first order. Using this property and making use of 1969 Mariner infrared spectrometer pressure measurements (Herr *et al.*, 1970) to normalize constants describing the ultraviolet atmospheric and surface scattering properties, pressures were measured at 337 points on the surface of Mars. Reflectance measurements of Mars at 3050 Å have been obtained by the Mariner 9 ultraviolet spectrometer during the time period 14 November 1971–1 March 1972.

When Mariner 9 arrived at Mars in November, the occurrence of a planet-wide dust storm prevented ultraviolet pressure measurements at the beginning of the mission. The net effect of the dust storm was to divide the 3050-Å reflectance measurements into two extremely opposite types of data. During the dust storm which lasted until about 1 January 1972, as observed in the ultraviolet, the 3050-Å reflectance of Mars was dominated by an optically thick and highly absorbing dust layer. From 23 January 1972 the Mars atmosphere was clear and the 3050-Å wavelength was optically thin, permitting ultraviolet pressures to be measured. In between these extremes, the atmosphere of Mars gradually became transparent. Measurements made in Hellas as late as 14 January 1972 indicated a sizable

amount of ultraviolet obscuration compared with clearer observations made later in the mission on 22 February 1972 and with similar observations made by Mariner 7 on 4 August 1969. Hellas may be obscured even when the remainder of the planet is clear (Sagan, Veverka, and Gierasch, 1971; Parkinson and Hunten, 1972).

The characteristics of the Mariner 9 ultraviolet spectrometer are discussed by Barth *et al.* (1972*b*). A field of view 0°.17 by 0°.48 gave a nominal 10 × 30 km field of view at a slant distance of 3400 km. During the 14 November 1971–1 March 1972 primary data-taking period, about 250 000 spectra of the illuminated disk of Mars were obtained. Of this number, 80% were obtained on the even-numbered orbits when Mars was in view of the 210-ft radio antenna at Goldstone, California. On one of these typical Goldstone zenith orbits, approximately 100 min of spectrometer data with Mars in view were transmitted to earth in real time. Since one complete spectrum was obtained every 3 sec, about 2000 individual reflectance measurements of Mars at 3050 Å were returned in real time each day. Results presented here are based upon a rapid preliminary analysis of the Mariner 9 ultraviolet spectrometer data carried out at the University of Colorado in near real time using preliminary orbital and instrument pointing information. This preliminary look at the entirety of the 3050-Å reflectance data, obtained from November to March, provides a characterization of Mars in the ultraviolet.

Dust Observations

The equation

$$R = \frac{p(\Psi)\tilde{\omega}_0\tau}{4\mu}\left[\frac{1-\exp(-\tau m)}{\tau m}\right] + R_0\frac{(\mu\mu_0)^k}{\mu}\exp(-\tau m) \qquad (1)$$

represents a general model for the reflectance of Mars, having validity whenever multiple-scattering effects are small and when the Minnaert function $R_0(\mu\mu_0)^k/\mu$ adequately represents the ground scattering. Reflectance R is the measured intensity divided by the solar flux at Mars and multiplied by π. In Eq. (1), $p(\Psi)$ is the scattering phase function normalized to have an average value of unity,

$$\frac{1}{4\pi}\int p(\Psi)\,d\Omega = 1. \qquad (2)$$

The effective single-scattering albedo or probability of reemission of a photon absorbed in the Mars atmosphere is $\tilde{\omega}_0$. Vertical optical thickness in the Mars atmosphere, assumed to be homogeneous, is represented by τ. In addition to the scattering angle Ψ two additional angles are needed to give a unique scattering geometry. These angles are the solar incidence and viewing emission angles measured with respect to the surface normal, assumed to be a Mars radius vector in this discussion. The incidence and emission angles are represented here by their cosines, μ_0 and μ. Air mass, the equivalent number of vertical optical paths traversed by a photon incident from the sun and scattered by the surface into the instrument field of view, is given by $m = 1/\mu + 1/\mu_0$.

Dust storm measurements at 3050 Å may be described by Eq. (1), where the reflectance approaches

$$R = \frac{p(\Psi)\tilde{\omega}_0}{4}\frac{\mu_0}{\mu+\mu_0} \qquad (3)$$

as τ becomes larger than unity. This result can also be obtained by representing the solution in terms of X and Y functions (Chandrasekhar, 1960) and considering the case of small single scattering probability, $\tilde{\omega}_0$. As τ becomes larger than unity, the X and Y function solution rapidly approaches the H-function solution, applicable for a semiinfinite atmosphere. Equation (3) represents the limiting case of an H function solution as $\tilde{\omega}_0$ becomes less than unity, or equivalently, when the effect of multiple scattering becomes negligible. The small reflectances observed by the Mariner 9 ultraviolet spectrometer as well as the small geometric albedos recorded by Earth-based ultraviolet measurements (e.g. Irvine *et al.*, 1968) imply that secondary and all

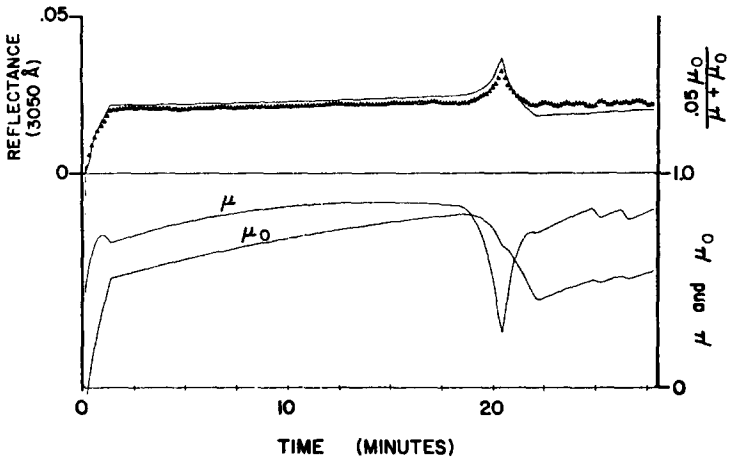

FIG. 1. Reflectance at 3050 Å as a function of time for part of data obtained on 20 December 1971. Geometry parameters μ_0 and μ, the cosines of the incidence and emission angles, are shown in the bottom half of the figure. A small value of μ indicates an observation made near the planet limb while a value of 1 indicates vertical viewing of Mars. Observations having small values of μ_0 are taken near the terminator. The value of μ_0 approaches 1 as data are obtained closer to the subsolar point. A nominal dust model is plotted as a solid line in the top half of the figure. Note that the model overestimates the reflectance up to time = 20 min and underestimates it after that. This is a result of a change in scattering angle Ψ from 112° to 137°.

higher orders of scattering contribute very little to the total intensity or reflectance. Effects of particle shadowing (Irvine, 1966) are not considered in this analysis. Under these conditions, the single particle scattering efficiency, $p(\Psi)\tilde{\omega}_0$, of the dust particles is being measured with little or no sensitivity to optical thickness, τ. A value of $p(\Psi)\tilde{\omega}_0 = 0.2$ models the bulk of reflectance measurements made during the 13 November 1971–1 January 1972 time period. A small dependence on scattering angle, Ψ, is noted in the data but is not reported on here. Mariner 9 made observations for values of Ψ ranging from 96° to 165°.

Figures 1–4 show examples of dust storm measurements obtained during the 13

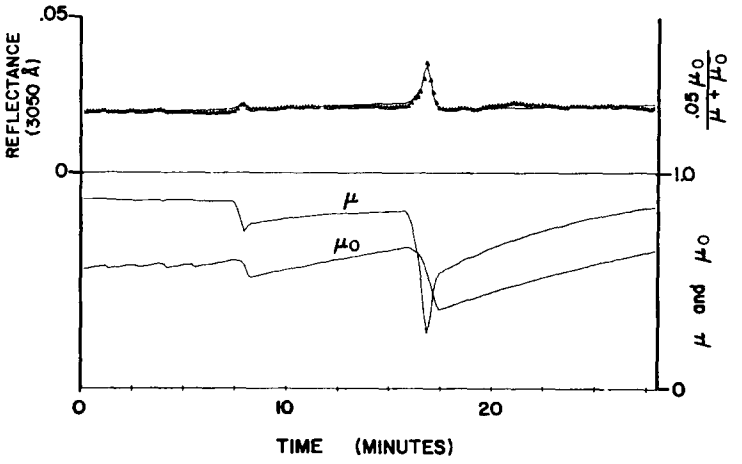

FIG. 2. Reflectance at 3050 Å, μ_0, μ, and the nominal dust model for part of data taken on 22 December 1971. The scattering angle changes from 133° to 147° at time = 17 min. Abrupt changes in μ and μ_0 occur when the pointing direction of the instrument platform is changed.

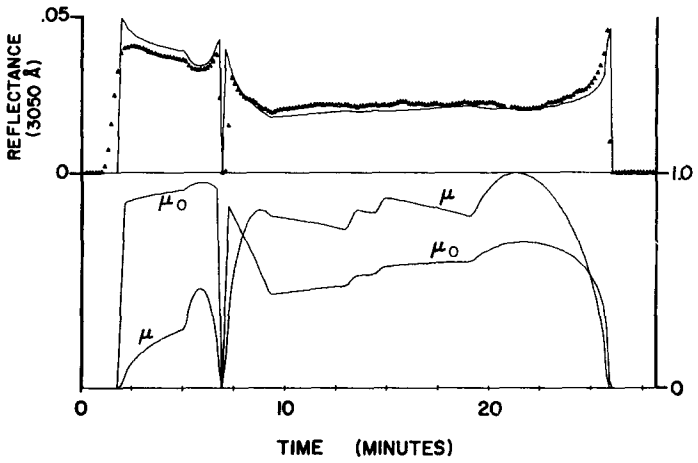

FIG. 3. Reflectance at 3050 Å, μ_0, μ, and the nominal dust model for part of data obtained on 23 December 1971. A complicated pointing sequence begins with the instrument field of view crossing the bright limb of Mars near the subsolar point. This sequence ends with the field of view leaving the planet at time = 26 min.

November 1971–1 January 1972 time period. These figures were taken from an early University of Colorado data report (Barth *et al.*, 1972*a*). Each 3050-Å datum point represents the average of data obtained from three successive spectra. Using this data contraction gives a more nearly square sampling area on the surface of Mars and does not degrade the data except near the planet limb or terminator. In Figs. 1–4, the agreement between a nominal model, $0.05\ \mu_0/(\mu + \mu_0)$, represented by a solid line, and the 3050-Å reflectance is shown. The effect of the third geometry parameter Ψ is shown here qualitatively. Increasing the scattering angle Ψ increases the observed reflectance while still following the $\mu_0/(\mu + \mu_0)$ dependence on incidence and emission angles. Limitations in the comparison of this model with the observed reflectance occur near the limb (small values of μ) or terminator (small values of μ_0) where the plane-parallel representation of a curved atmosphere fails. Variations with latitude and longitude did not appear in the data due to the global nature of the dust storm. Increased brightness near the morning

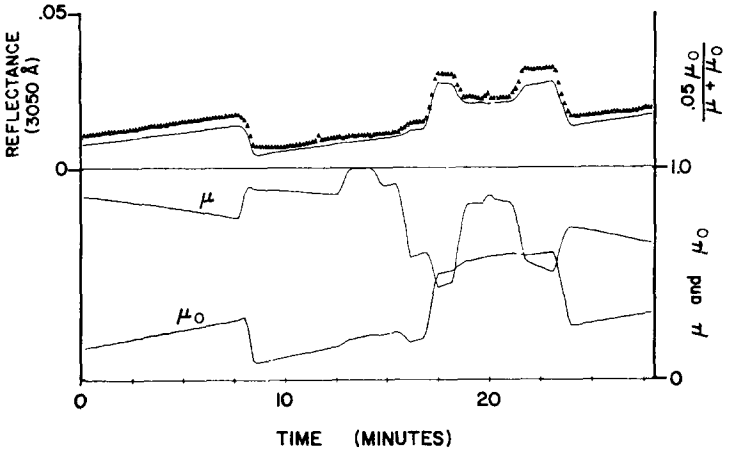

FIG. 4. Reflectance at 3050 Å, μ_0, μ, and nominal dust model as a function of time for part of data taken on 26 December 1971.

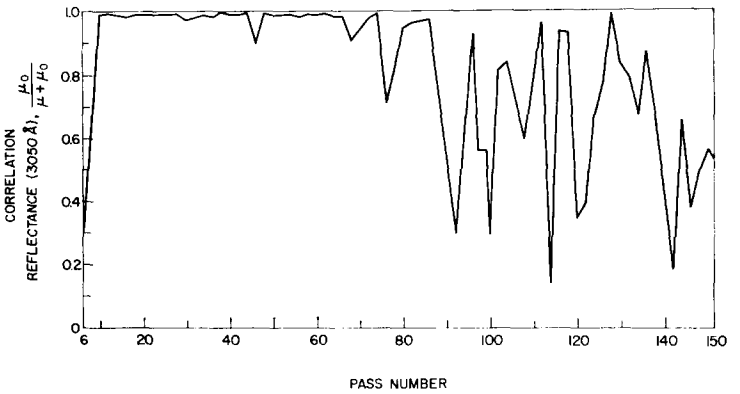

FIG. 5. Results of regression to find out how well measured reflectance is predicted by the dust model functional dependence, $\mu_0/(\mu + \mu_0)$.

terminator and at extreme southerly latitudes was observed. The increase in brightness near the morning terminator may represent a condensate formed during the previous night. The south polar cap was clearly seen in the ultraviolet during the dust storm (Barth *et al.*, 1972*b*; Lane, 1972), indicating the atmosphere was clearer at southerly latitudes. Pang (1971) has estimated the optical thickness of the dust in the polar cap region to be of order unity based upon the variation of polar cap brightness with absorption airmass.

Figure 5 shows the correlation of the 3050-Å reflectance data with the function $\mu_0/(\mu + \mu_0)$, from Eq. (3), for the even-numbered Mariner 9 orbits 6–150. For each orbit in this sequence, a correlation was performed for a single scattering angle Ψ. The number of points, each formed from an average of three spectra, varied from 70 to 200. Measurements having large emission or incidence angles, μ or $\mu_0 < 0.3$, were rejected from these regressions. The demise of the dust storm is evident in Fig. 5 where a transition from a correlation coefficient near unity begins after orbit 80, 25 December 1971, to smaller values as clear conditions are approached and local topography begins to control the ultraviolet intensity.

SURFACE PRESSURE

After the dust storm subsided, a large amount of 3050-Å data were obtained providing ultraviolet information about Mars under the characteristically clear conditions seen by Mariner 6 and 7 in 1969. The small surface albedo of Mars in the ultraviolet causes the atmospheric scattering signal to make up a substantial part of the observed intensity. Under these conditions Rayleigh scattering from the molecular CO_2 atmosphere dominates the fluctuations in the 3050-Å reflectance, providing a measure of surface pressure. Since the Mars atmosphere is optically thin, the measured intensity is proportional to the vertical optical thickness τ which is, in turn, proportional to the vertical column density of molecules above the planet surface. The surface pressure is that required to support this column of molecules in the Mars gravitational field, independent of atmospheric temperature structure.

Residual dust is assumed to be fine and have a long settling time in the Mars atmosphere, and therefore tends to be uniformly mixed with the molecular atmosphere. The presence of a homogeneously mixed dust would not affect the pressure measuring concept but would cause the atmospheric scattered intensity to differ from that expected from a pure molecular atmosphere. In order to establish a pressure model under these conditions, comparisons are made with pressures measured by the Mariner 9 radio occultation experiment (Kliore *et al.*, 1972).

For the preliminary presentation of

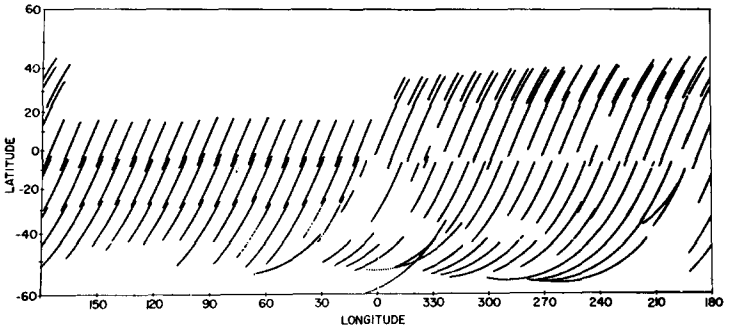

FIG. 6. Location in latitude and longitude of 3050-Å reflectance measurements used to construct pressure—altitude map of Mars.

Mariner 9 ultraviolet pressure mapping given here, a simplified form of Eq. (1) is used. The effect of atmospheric absorption is neglected and the phase function is assumed to be of the form

$$p(\Psi) = \alpha(1 + \beta \cos^2 \Psi), \qquad (4)$$

where β is a parameter to be determined and α is fixed by the normalization, Eq. (2). Using this form for $p(\Psi)$ allows for polarization effects in the instrument. A more complicated phase function with more parameters was not felt to be justified in this preliminary analysis. If these assumptions are made, Eq. (1) may be written in a form suitable for comparison with the Mariner 9 radio occultation measurements,

$$(1 + \beta \cos^2 \Psi)P = A\mu R - B(\mu\mu_0)^k. \qquad (5)$$

Pressure P is proportional to optical thickness τ in Eq. (1). Four parameters, β, A, B, and k, are to be determined through comparison of the occultation pressure P with the ultraviolet reflectance R obtained while viewing the occultation measurement locations on Mars. Ultraviolet reflectance measurements are made at a known geometry described by Ψ, μ, and μ_0. Parameters A and B translate into values for single scattering albedo, $\tilde{\omega}_0$, and the Minnaert constant R_0. Two of the parameters to be determined are associated with atmospheric properties, $\tilde{\omega}_0$ and β, and two with the surface, R_0 and k.

The ultraviolet data used in this analysis were obtained in the time period from 23 January 1972 to 1 March 1972. During this time, 39 orbits of spectrometer data were obtained while the Mars atmosphere was clear. About 800 of the spectra obtained each day were in the Mars afternoon extending from −50° South to 15° or 30° North with the viewing track running toward the northeast. These afternoon measurements encircle Mars with swaths of measurements 9° apart in longitude. Figure 6 shows a graph of afternoon data swaths on a Mercator projection. The location of every third spectral measurement is plotted. Reflectance measurements used in this analysis are restricted to those obtained when μ and $\mu_0 > 0.3$. Locations of ultraviolet measurements obtained during orbits 150–216 were searched to find data within 3° of an occultation measurement. The closest measurement from each ultraviolet viewing swath was selected for comparison. Early results made available by the Mariner 9 radio occultation experimenters (Kliore *et al.*, 1972) for this comparison are listed in Table I. In principle, only four comparison points are necessary to specify parameters β, $\tilde{\omega}_0$, R_0, and k. Because of measurement uncertainties coupled with known differences in the latitude and longitudes being compared, a least-squares adjustment of the four parameters was made using all 56 comparison points. No allowance was made for differences in the areas of Mars sampled by the two methods, and none of the comparison points were rejected. Results of the least-squares adjustment indicated that a sizable range of matched sets of parameters β, $\tilde{\omega}_0$, R_0, and k did not alter

TABLE I

MARINER 9, PRESSURE COMPARISON

P(UV)	P(OCC)	Diff.	UV Orbit	OCC Orbit	Lat.	Lon.	Location
3.6	4.3	−0.7	150	2	−39.9	142.8	M. Sirenum
4.0	4.4	−0.4	150	6	−38.2	140.4	M. Sirenum
3.8	4.4	−0.6	152	6	−38.2	140.4	M. Sirenum
3.9	4.1	−0.2	152	2	−39.9	142.8	M. Sirenum
4.4	4.1	0.3	154	2	−39.9	142.8	M. Sirenum
4.9	3.5	1.4	156	8	−37.6	130.6	Sirenum S.
4.6	4.1	0.5	156	10	−36.3	120.8	Icaria
2.4	2.9	−0.5	156	49	−13.3	107.8	Phoenicis L.
4.4	3.6	0.8	158	12	−35.4	110.9	Daedalia
2.8	2.8	0.0	160	14	−34.5	100.8	Claritas
5.0	3.6	1.4	160	12	−35.4	110.9	Daedalia
3.7	2.8	0.9	160	14	−34.5	100.8	Claritas
3.4	3.4	0.0	160	53	−10.1	88.1	Tithonius L.
3.6	3.4	0.2	162	16	−33.5	90.7	Solis L.
3.2	3.5	−0.3	164	18	−32.5	80.5	Solis L.
3.1	3.4	−0.3	164	16	−33.5	90.7	Solis L.
2.6	2.8	−0.2	164	14	−34.5	100.8	Claritas
3.6	3.5	0.1	164	18	−32.5	80.5	Solis L.
6.4	4.4	2.0	166	6	−38.2	140.4	M. Sirenum
3.3	3.8	−0.5	166	20	−31.4	70.3	Thaumasia
4.1	4.2	−0.1	166	59	−4.7	58.4	Juventae Fons
3.8	4.2	−0.4	168	22	−30.3	60.1	Nectar
3.6	4.2	−0.6	168	22	−30.3	60.1	Nectar
5.0	4.7	0.3	170	24	−29.2	49.9	M. Erythraeum
5.0	4.7	0.3	170	24	−29.2	49.9	M. Erythraeum
4.4	4.9	−0.5	174	28	−27.0	29.7	Pyrrhae R.
5.5	4.9	0.6	174	28	−27.0	29.7	Pyrrhae R.
5.4	4.9	0.5	174	28	−27.0	29.7	Pyrrhae R.
5.2	5.5	−0.3	176	30	−25.8	19.7	Pyrrhae R.
5.2	5.5	−0.3	178	30	−25.8	19.7	Pyrrhae R.
5.2	5.5	−0.3	178	30	−25.8	19.7	Pyrrhae R.
5.1	5.5	−0.4	178	30	−25.8	19.7	Pyrrhae R.
5.9	5.5	0.4	182	30	−25.8	19.7	Pyrrhae R.
5.3	5.5	−0.2	182	30	−25.8	19.7	Pyrrhae R.
5.3	5.5	−0.2	182	30	−25.8	19.7	Pyrrhae R.
5.2	5.5	−0.3	182	30	−25.8	19.7	Pyrrhae R.
4.7	4.9	−0.2	184	32	−24.6	9.9	Pyrrhae R.
4.0	4.6	−0.6	186	36	−22.1	350.4	Pandorae Fr.
4.2	4.4	−0.2	190	3	−39.5	326.5	Hellespontus
3.5	4.4	−0.9	192	3	−39.5	326.5	Hellespontus
4.6	5.0	−0.4	194	7	−37.7	315.5	Yaonis Fr.
9.6	8.7	0.9	200	13	−35.0	285.8	Hellas
6.8	8.7	−1.9	200	13	−35.0	285.8	Hellas
7.8	6.8	1.0	202	15	−34.0	275.8	M. Hadriacum
7.5	6.8	0.7	202	15	−34.0	275.8	M. Hadriacum
7.0	6.8	0.2	202	15	−34.0	275.8	M. Hadriacum
7.0	6.8	0.2	202	15	−34.0	275.8	M. Hadriacum
5.4	5.0	0.4	204	58	−5.7	243.3	Tritonis S.
4.9	4.7	0.2	208	21	−30.9	245.2	M. Tyrrhenum
5.0	4.6	0.4	208	19	31.9	255.4	Ausonia

TABLE I—*continued*

P(UV)	*P*(OCC)	Diff.	UV Orbit	OCC Orbit	Lat.	Lon.	Location
5.5	6.3	−0.8	208	62	−1.8	223.4	Aeolis
5.2	6.4	−1.2	210	64	0.3	213.8	Aeolis
5.1	4.3	0.8	212	25	−28.7	224.9	Hesperia
5.4	7.1	−1.7	214	68	5.1	195.1	Mesogaea
6.3	4.3	2.0	216	25	−28.7	224.9	Hesperia
5.2	4.3	0.9	216	29	−26.4	204.7	M. Cimmerium

the pressure residuals, or differences between ultraviolet and occultation pressures, by a significant amount. Because of location uncertainties which will be resolved as final orbital pointing information becomes available, an intermediate method was used to scale the ultraviolet pressures. This method was to allow $\tilde{\omega}_0$, R_0, and k to be selected by comparison with occultation measurements and to select a value of β which provided self-consistent values for separate ultraviolet measurements made at the same location on Mars. Figure 7 indicates the values of the cosines of the incidence and emission angles, μ and μ_0, for the comparison points. Figure 8 shows a plot of μR against $\mu\mu_0$ on a logarithmic scale. The effect of atmospheric scattering on the measured reflectance is evident as points having occultation pressures higher than 6.5 mbar are seen to lie above the centroid of the data while those for pressures less than 3.5 mbar lie below. Figure 9 shows a plot of μ multiplied by the reflectance attributed to the planet surface, $R - p(\Psi)\tilde{\omega}_0\tau/(4\mu)$, against $\mu\mu_0$. The dispersion in the data of Fig. 8 is largely accounted for by a correction for atmospheric scattering used in Fig. 9. Improvement brought about by final orbital pointing information is expected to reduce the remaining dispersion shown in Fig. 9. Table I lists the ultraviolet and radio occultation pressures and differences at the 56 comparison points.

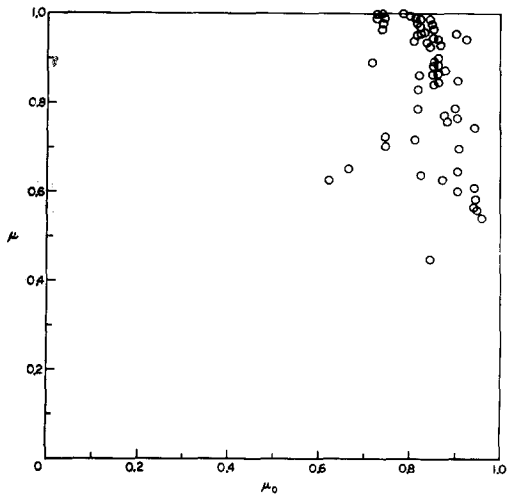

FIG. 7. Distribution of ultraviolet/radio occultation comparison points according to the cosines of incidence and emission angles, μ_0 and μ.

Some results are obtained which are relatively insensitive to the particular values of the parameters β, $\tilde{\omega}_0$, R_0, and k. The ultraviolet and radio occultation pressures have a root mean square difference of 16% over the 2.6–8.1 mbar pressure range of the radio occultation comparison points. In Eq. (5) the term attributable to scattering from the surface of Mars, $B(\mu\mu_0)^k$, is 50–60% of the total reflectance term, $A\mu R$, averaged over the comparison points. This result is consistent with some earlier estimates (e.g. Caldwell, 1970).

A preliminary ultraviolet pressure altitude contour map of Mars is shown in Fig. 10. The altitudes have been computed from pressures assuming an atmosphere having a scale height of 10 km, corresponding to an effective temperature of 190 K. The zero altitude level is taken as the

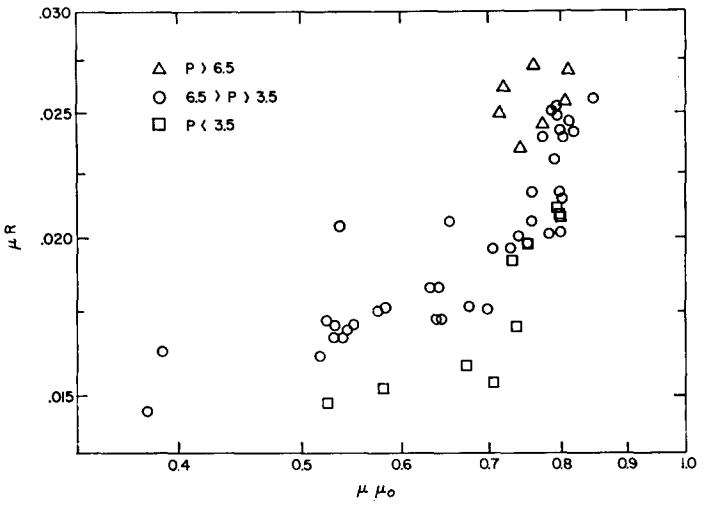

FIG. 8. A Minnaert plot of ultraviolet reflectance for 56 occultation comparison points. The ordinate is the 3050-Å reflectance multiplied by the cosine of the emission angle, μ. The abscissa is the product of the cosines of the incidence and emission angles, $\mu_0\mu$. If the Mars atmosphere were absent, and the planet surface were correctly represented by a Minnaert function, $R_0(\mu\mu_0)^k$, the data would cluster along a straight line of slope k and have an intercept at R_0. The effect of atmospheric scattering disperses the data along the ordinate depending on the local pressure.

triple point pressure of water, 6.1 mbar. A total of 30 000 individual 3050-Å measurements were used. These measurements have been smoothed to a 10° grid to show the large-scale pressure altitude variations on Mars. It should be noted that Earth-based radar topographic measurements cannot be compared directly with these measurements. Ultraviolet pressure altitudes are references with respect to an

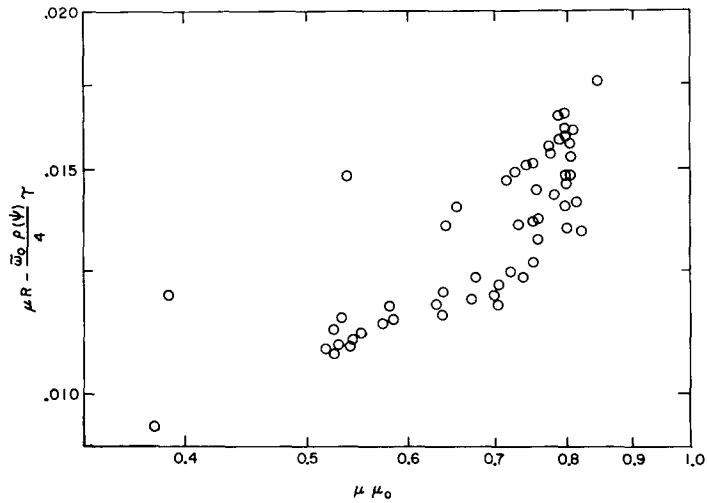

FIG. 9. A Minnaert plot, similar to Fig. 8 with the dispersion due to atmospheric scattering removed. The trend of the data indicate that a more sophisticated model for the ground reflectance in terms of geometry, μ, μ_0, and Ψ may be needed.

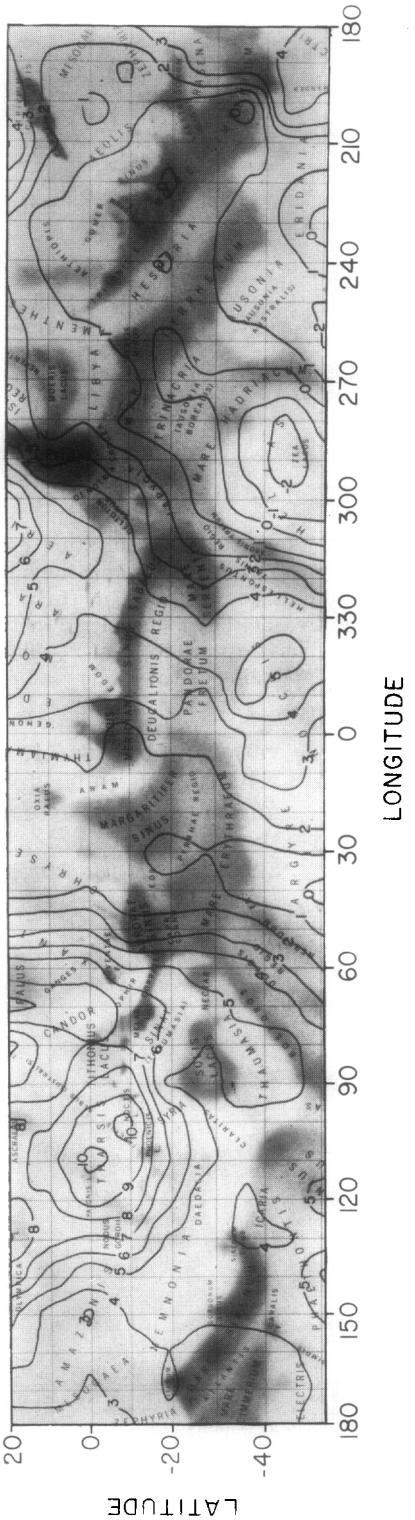

FIG. 10. Preliminary ultraviolet pressure–altitude contour map of Mars smoothed to 10° in longitude and latitude, as measured near the equator. The Mercator contour plot is overlaid on a Mariner 9 planning map prepared by de Vaucouleurs. The high at the top of the map at 130° west longitude is due to Nix Olympica. The relative high at 100° west and 0° latitude represents the center of the North, Middle, and South Spot volcano group, while the second high south and east is at the beginning of the large Mars riftlike feature which terminates just west of the relative low at 35° west and 20° south. The volcanic region in Elysium is a relative high at the top of the map at 210° west longitude. Hellas is the low at 290° west longitude and −45° latitude.

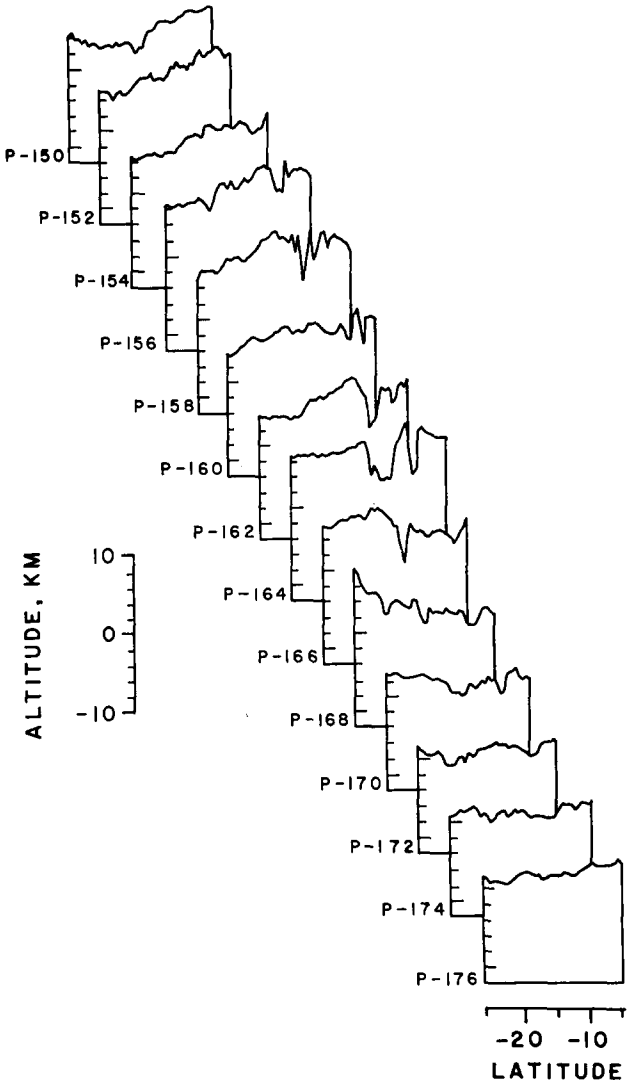

FIG. 11. Detailed ultraviolet pressure altitude sections across the Mars rift region.

equipotential surface, while radar measurements (Downs *et al.*, 1972; Pettengill *et al.*, 1972) represent distances measured from the center of Mars. Results from the Mariner 9 celestial mechanics experiment (Lorell *et al.*, 1972) and the radio occultation experiment (Cain *et al.*, 1972) indicate that the Mars gravitational field has large deviations from spherical symmetry. Because of these gravitational variations, it is necessary for radar measurements to be translated, making use of a correct gravitational field model, in order to determine pressure altitudes or which direction water would flow, for example.

In addition to analysis of the Mars pressure altitude from a global point of view, very detailed information was obtained along the path of the spectrometer viewing track. One of the most striking changes in pressure altitude occurs over the Tharsis region where the Mariner 9 television pictures show a large riftlike

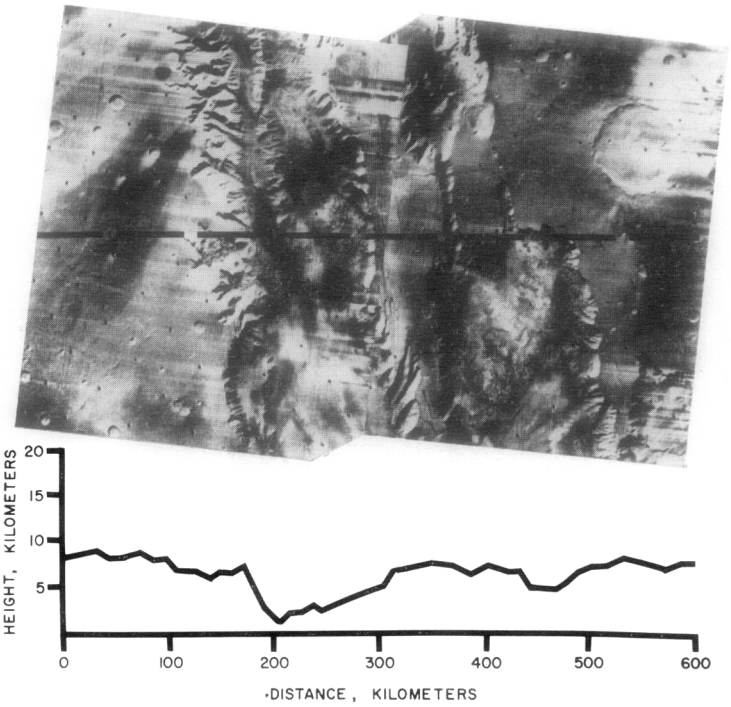

FIG. 12. Ultraviolet pressure altitude profile across the rift region shown with Mariner 9 television pictures of the same region.

feature running 50° in longitude from west to east (McCauley *et al.*, 1972). Figure 11 shows detailed pressure altitudes measured in the Tharsis region during the time period from 28 January to 10 February 1972. The ultraviolet pressure altitude swaths cross the rift feature in a nearly perpendicular manner. The sequence of data swaths begins at 140° west, orbit 150, and extends about 7500km east to a longitude of 5° west, orbit 176. Each detailed mapping swath extends for 1200 km. The west edge of the canyon begins on a dome in the Tharsis region and was crossed on orbit 156, as shown in Fig. 11. Pressure altitudes, starting with the highest point along orbit 150, 6km, increase to a maximum of 9km, measured on orbit 156 near the beginning of the rift feature. From this dome the altitude decreases going eastward, reaching a minimum of −0.5km on orbit 172 at 30° west longitude in Margaritifer Sinus. At its widest point, recorded on orbit 164, the rift depth is 6km.

The high degree of detail along the mapping swaths was utilized to make a detailed point-by-point comparison with television pictures supplied by the Mariner 9 television experimenters (McCauley *et al.*, 1972). Fourteen individual spectral measurements were obtained across each wide-angle television picture and relative altitudes associated with these pictures were recorded daily during the mission. Figure 12 shows the detailed ultraviolet pressure altitude profile from orbit 164 across the rift together with Mariner 9 television pictures. The other features on Mars which show large changes in pressure elevation are the volcanos, Nix Olympica and North, Middle, and South Spots (McCauley *et al.*, 1972). Figure 13 shows the detailed pressure altitude profile across Middle Spot. It is notable that the caldera does not occur at the summit. The large

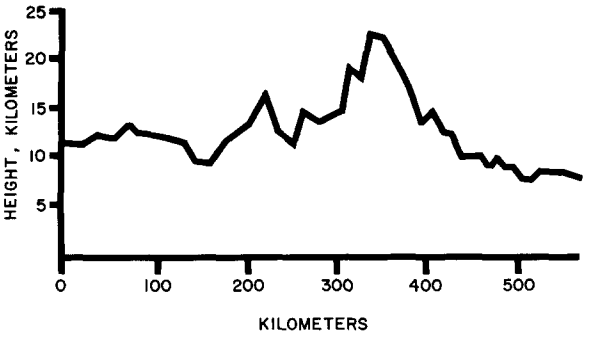

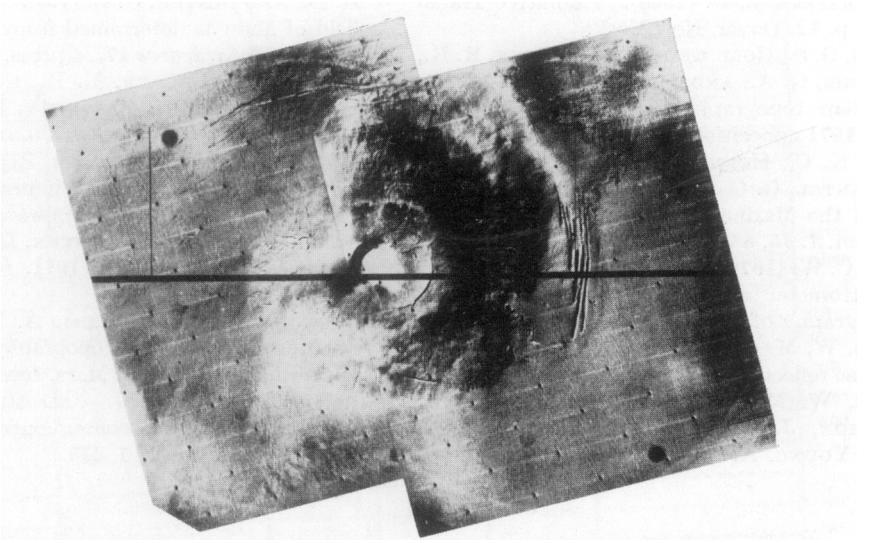

FIG. 13. Pressure altitude profile of Middle Spot measured on 1 February 1972 shown with accompanying television pictures.

altitude of Middle Spot relative to its surroundings nearly 15km made it, along with other volcanos, visible during the early part of the mission when dust obscured the rest of the planet.

Note added in proof. It has been brought to our attention by A. J. Kliore that the ultraviolet pressures are systematically low compared with radio occultation measurements in the northerly latitudes. Requiring radio occultation comparison points to be within 3° of an ultraviolet measurement excluded a number of possible occultation anchor points in the northeastern part of the map shown in Fig. 10. When the comparison points are required to be within 5°, rather than 3°, so that these northerly points may be included, then ultraviolaet pressure altitudes north of 0° latitude are systematically lowered.

ACKNOWLEDGMENTS

We thank Karen Simmons, Lois McLaughlin, Randy Davis, and Mary Dick who made valuable contributions in the computer preparation of the data.

This work was supported by the National Aeronautics and Space Administration.

REFERENCES

BARTH, C. A., AND HORD, C. W. (1971). Mariner ultraviolet spectrometer: Topography and polar cap. *Science* **173**, 197–201.

BARTH, C. A., HORD, C. W., STEWART, A. I., AND LANE, A. L. (1972*a*). Mariner 9 Mars orbiter ultraviolet spectrometer experiment:

Data report 4. Laboratory for Atmospheric and Space Physics, University of Colorado, February 2.

BARTH, C. A., HORD, C. W., STEWART, A. I., AND LANE, A. L. (1972*b*). Mariner 9 ultraviolet spectrometer experiment: Initial report. *Science* **175**, 309–312.

CAIN, D. L. (1972). The shape of Mars from Mariner 9 occultations. *Icarus* **17**, in press.

CALDWELL, J. J. (1970). Ultraviolet observations of Mars made by the Orbiting Astronomical Observatory. Ph.D. Thesis, University of Wisconsin; also submitted to *Icarus*.

CHANDRASEKHAR, D. (1960). "Radiative Transfer." p. 12. Dover, New York.

DOWNS, G. S., GOLDSTEIN, R. M., GREEN, R. R., MORRIS, G. A., AND REICHLEY, P. E. (1972). Martian topography and radar brightness: The 1971 opposition. *Icarus* **17**, in press.

HERR, K. C., HORN, D., MCAFEE, J. M., AND PIMENTEL, G. C. (1970). Martian topography from the Mariner 6 and 7 infrared spectra. *Astron. J.* **75**, 833–894.

HORD, C. W. (1972). Mariner 6 and 7 ultraviolet spectrometer experiment: Photometry and topography of Mars. *Icarus* **16**, 253.

IRVINE, W. M. (1966). The shadowing effect in diffuse reflection. *J. Geophys. Res.* **71**, 2931.

IRVINE, W. M., SIMON, T., MENZEL, D. H., CHARON, J., LECOMTE, G., GRIBOVAL, P., AND YOUNG, A. T. (1968). Multicolor photoelectric photometry of the brighter planets. II. Observations from Lehouga Observatory. *Astron. J.* **73**, 251–264.

KLIORE, A. J., CAIN, D. L., FJELDBO, G., SEIDEL, B. L., SYKES, M. J., AND RASOOL, S. I. (1972). Atmosphere and topography of Mars from Mariner 9 radio occultation measurements. *Icarus* **17**, in press.

LANE, A. L. (1972). Ultraviolet observations of ozone on Mars. *Icarus* **17**, in press.

LORELL, J., BORN, G. H., CHRISTENSEN, E. J., JORDAN, J. F., LAING, P. A., MARTIN, W. L., SJOGREN, W. L., SHAPIRO, I. I., REASENBERG, R. D., AND SLATER, G. L. (1972). The gravity field of Mars as determined from Mariner IX tracking data. *Icarus* **17**, in press.

MCCAULEY, J. F., CARR, M. H., CUTTS, J. A., HARTMANN, W. K., MASURSKY, H., MILTON, D. J., SHARP, R. P., AND WILHELMS, D. E. (1972). Preliminary Mariner Report on the Geology of Mars. *Icarus* **17**, in press.

PANG, K. D. (1971). Private communication.

PARKINSON, T. D., AND HUNTEN, D. M. (1972). CO_2 mapping of Mars in 1971. *Icarus* **17**, in press.

PETTENGILL, G. H., ROGERS, A. E. E., AND SHAPIRO, I. I. (1972). Topography and radar scattering properties of Mars. *Icarus*, in press.

SAGAN, C., VEVERKA, J., AND GIERASCH, P. (1971). Observational consequences of Martian wind regime. *Icarus* **15**, 253.